AFRL-AFOSR-VA-TR-2019-0068

Nonreciprocal Metal-Dielectric Photonic Structures for Electromagnetic Isolation and Power Control

ANDREY CHABANOV
University of Texas at San Antonio

03/07/2019
Final Report

Air Force Research Laboratory
AF Office Of Scientific Research (AFOSR)/ RTB1
Arlington, Virginia 22203
Air Force Materiel Command

REPORT DOCUMENTATION PAGE

Form Approved
OMB No. 0704-0188

1. REPORT DATE *(DD-MM-YYYY)*	2. REPORT TYPE	3. DATES COVERED *(From - To)*
15-03-2019	Final Performance	01 Dec 2015 to 30 Nov 2018

4. TITLE AND SUBTITLE
Nonreciprocal Metal-Dielectric Photonic Structures for Electromagnetic Isolation and Power Control

5a. CONTRACT NUMBER

5b. GRANT NUMBER
FA9550-16-1-0058

5c. PROGRAM ELEMENT NUMBER
61102F

6. AUTHOR(S)
ANDREY CHABANOV

5d. PROJECT NUMBER

5e. TASK NUMBER

5f. WORK UNIT NUMBER

7. PERFORMING ORGANIZATION NAME(S) AND ADDRESS(ES)
University of Texas at San Antonio
One Utsa Circle
San Antonio, TX 78249-1130 US

8. PERFORMING ORGANIZATION REPORT NUMBER

9. SPONSORING/MONITORING AGENCY NAME(S) AND ADDRESS(ES)
AF Office of Scientific Research
875 N. Randolph St. Room 3112
Arlington, VA 22203

10. SPONSOR/MONITOR'S ACRONYM(S)
AFRL/AFOSR RTB1

11. SPONSOR/MONITOR'S REPORT NUMBER(S)
AFRL-AFOSR-VA-TR-2019-0068

12. DISTRIBUTION/AVAILABILITY STATEMENT
A DISTRIBUTION UNLIMITED: PB Public Release

13. SUPPLEMENTARY NOTES

14. ABSTRACT
This research project has developed RF composite materials which are capable of dramatically enhancing essential magnetophotonic responses, such
as Faraday rotation, while drastically reducing absorption losses. The composites also provide qualitatively new features, unattainable from uniform
magnetic materials, such as wide-aperture, omnidirectional isolation. The developed isolator design is based on a multilayered structure hosting a
ferromagnetic nanolayer and a set of dichroic layers, which is so thin that the entire structure can be bent and used to cover a wide area with an
arbitrary shape. The key structural elements, the ultra-thin Faraday rotator and absorptive sheet polarizers, have been successfully tested at X- and
W-band frequencies.
Furthermore, multilayered structures with phase-change components, such as vanadium dioxide, have been shown to perform as a reflecting
photonic limiter in the W-band, transmitting low-intensity radiation while totally reflecting radiation with intensity exceeding a certain limiting
threshold. In the developed multilayers, the limiting threshold for the forward propagating radiation can differ widely from that for the backward

15. SUBJECT TERMS
magneto-optical, Q-factor, Quality factor, ferromagnets, resonance, losses, lossy, birefringence, circular birefringence, composite

16. SECURITY CLASSIFICATION OF:			17. LIMITATION OF ABSTRACT	18. NUMBER OF PAGES	19a. NAME OF RESPONSIBLE PERSON
a. REPORT	b. ABSTRACT	c. THIS PAGE			SAYIR, ALI
Unclassified	Unclassified	Unclassified	UU		19b. TELEPHONE NUMBER *(Include area code)* 703-696-7236

DISTRIBUTION A: Distribution approved for public release

Nonreciprocal Metal-Dielectric Photonic Structures for Electromagnetic Isolation and Power Control

Final Report

Andrey Chabanov (University of Texas – San Antonio)

It is well known that an effective way to drastically enhance light-matter interaction is to incorporate the optical material into a complex photonic structure with feature sizes comparable to the light wavelength in the medium [1]. Such photonic structures with engineered dispersion can display unique optical properties unattainable from uniform (single-phased) optical materials. In properly designed photonic structures supporting slow-waves or cavity resonances, light-matter interaction can be enhanced by several orders of magnitude compared to that of uniform optical components. Such enhancement can lead to a dramatic size reduction and performance improvement. Particularly efficient can be photonic structures with engineered spectral singularities associated with slow light propagation [2,3] and arrays of optical resonators [4-9]. A common problem with either approach, however, is that the same slow-light or resonance conditions can also cause the enhancement of absorption, which increases energy losses, heating, etc. [10-12] In addition, the enhanced absorption can dramatically lower the Q-factor of the optical resonance and, because of that, significantly compromise the component performance as the enhancer of the useful light-matter interaction [13].

In the reported research effort, we have developed photonic structures in which only targeted property of the functional material (e.g., magnetic, nonlinear, phase-change, etc.) is enhanced, whereas losses and/or other unwanted light-matter interactions are kept limited, or even reduced. As has been proposed, we have focused on magnetic materials that break time-reversal symmetry of EM wave propagation, providing critical functionalities such as optical isolation and circulation in RF systems. The developed MW isolator is based on a multilayered structure hosting a ferromagnetic nanolayer and a set of dichroic layers, which is so thin that the entire structure can be bent and used to cover a wide area with an arbitrary shape. The key structural elements, the ultra-thin Faraday rotator and absorptive sheet polarizers, have been developed and successfully tested at X- and W-band frequencies [14,15]. In addition, we have designed multilayered structures with phase-change components, such as vanadium dioxide, acting as reflecting photonic limiters in the W-band [16]. The reflective photonic limiter transmits low-intensity radiation while totally reflecting radiation with intensity exceeding a certain limiting threshold. In the developed limiter designs, the limiting threshold for the forward propagating wave can differ widely from that for the backward propagating wave. Within the lower and the upper limits, the multilayer displays unidirectional transmittance, and therefore can act as a free-space MW isolator with extraordinary power-handling capabilities – exceeding those available with conventional magnetic isolators and circulators by orders of magnitude. In the following, we describe MW isolators with magnetic and phase-change components.

1. Free-space wide-aperture sheet-isolator based on a multilayered resonant cavity

A typical free-space isolator comprises a 45-degree Faraday rotator (FR) placed between a pair of linear polarizers (LSP1 and LSP2) with 45-degree misalignment, as schematically shown in Fig. 1 [17]. The existing free-space isolators have certain inherent problems, one of which is a limited aperture. In the reported research we explore the possibility of a (multilayered) sheet-isolator with

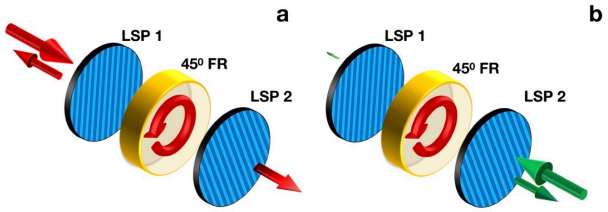

Fig. 1: Schematics of a free-space isolator consisting of 45⁰ Faraday rotator (45⁰FR) placed between two 45⁰ misaligned linear polarizers (LSP1 and LSP2): (a) forward propagating wave with TM polarization passes through; (b) backward propagating wave is blocked, regardless of its polarization.

virtually unlimited aperture. The latter requirement implies that both polarizers LSP1 and LSP2 in Fig. 1 should also be sheet-polarizers, as opposed to beam-splitting polarizers. A fundamental problem with the existing dichroic sheet-polarizers is that they only partially absorb the input light component with unwanted linear polarization, while the rest of it is reflected [18,19]. The partial reflectivity of the unwanted linear polarization will inevitably result in a failure of the sheet isolator. Indeed, the backward propagating input light (the one that should be blocked by the isolator), after entering the system through the polarizer LSP2 in Fig. 1b, will bounce back and forth between the two polarizers, every time passing through the Faraday rotator and acquiring additional 45-degree Faraday rotation. After two bounces, the light will return to the polarizer LSP1 with additional 90-degree polarization rotation and, thus, will not be blocked by the polarizer LSP1. The latter amounts to isolation failure. To prevent the backward propagating input light from passing through the sheet-isolator, we must make at least one of the two polarizers perfectly absorptive for the unwanted linear polarization, thereby, preventing the backward propagating input light from bouncing back and forth between the two polarizers. Designing perfectly absorptive sheet polarizers and incorporating them into the multilayered sheet isolator was one of the objectives of our investigation.

Here we report different sheet polarizers involving dichroic nanolayer(s) incorporated into the low-loss resonant cavity shown in Fig. 2a. In our simulations, the lossless resonant cavity involves a half-wave defect layer located in the middle of a periodic stack of alternating quarter-wave layers with the high (H) and the low (L) dielectric constant. The entire configuration can be described as $(HL)^4(LH)^4$. The constitutive layers of the resonant cavity have the respective dielectric constants of $\varepsilon_H = 9.5$ and $\varepsilon_L = 3.8$. The quarter-wave layers thicknesses are $d_H = \lambda_0/4\sqrt{\varepsilon_H}$ and $d_L = \lambda_0/4\sqrt{\varepsilon_L}$, respectively. The half-wave defect layer provides a quasi-localized mode associated with the resonant transmittance at the mid-gap wavelength of λ_0. Since the half-wave defect layer has the low refractive index, the resonant field distribution shown in Fig. 2b has antinodal plane in the middle of the defect layer, where the amplitude of the quasi-localized resonant mode reaches its maximum value. In our simulations we use the quarter-wave layer thicknesses of $d_H = 256$ nm and $d_L = 405$ nm, in which case the frequency

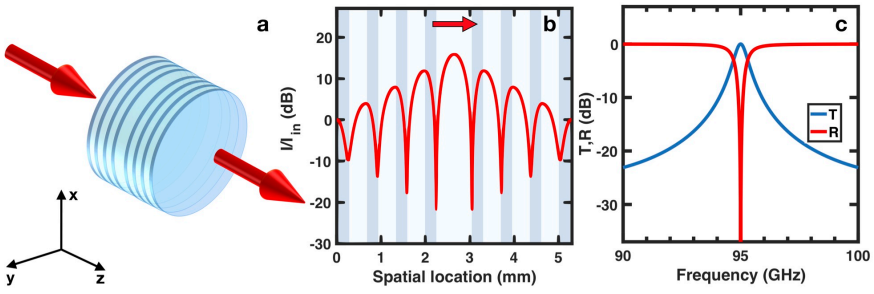

Fig. 2: (a) Schematics of the low-loss multilayered cavity $(HL)^4(LH)^4$ used as the host structure for the layered sheet polarizers (LSP) in Figs. 3 - 5; the light blue and the deep blue colors indicate the low (L) and the high (H) dielectric constants, respectively. (b) Simulated spatial intensity distribution, $|E(z)|^2$, at the cavity resonance frequency of 95 GHz. (c) Simulated dispersion spectra of the transmittance (T) and reflectance (R) in the vicinity of the cavity resonance. In the case of the low-loss resonant cavity in Fig. 2a, the plots in (b) and (c) are polarization independent. The plots (b) and (c) also apply to the cases of the LSP shown in Figs. 3a, 4a, and 5a, but only for the allowed (TM) polarization. In other words, the presence of dichroic nanolayers in those cases does not affect the transmission characteristics of the entire stack for the allowed linear polarization.

of resonant transmittance is 95 GHz. The calculated transmission dispersion of the resonant cavity (without dichroic nanolayers) is shown in Fig. 2c. The field distribution at the frequency of resonant transmission is shown in Fig. 2b. The addition of one or more (aligned) ultra-thin dichroic nanolayers to the resonant cavity does not affect the wave propagation with the desired linear polarization (hereinafter, the TM polarization) – the resonant field distribution and the transmission dispersion remain nearly the same as those shown in Figs. 2b and 2c for the case of the resonant cavity without the dichroic nanolayers. What happens to the undesired polarization component (hereinafter, the TE polarization) strongly depends on the location of the dichroic nanolayers in the resonant cavity. For instance, in the simplest symmetric configuration shown in Fig. 3, the incident wave with the TE polarization is nearly totally reflected. By contrast, in the more complex, but still symmetric configuration shown in Fig. 4, the input wave with the undesired TE polarization experiences a nearly total resonant absorption at the frequency of the cavity resonance. Finally, in the asymmetric configuration shown in Fig. 5, the wave with the undesired TE polarization experiences either strong broadband reflectivity (for the forward direction of incidence), or strong resonant absorption (for the backward direction of incidence), as shown in Fig. 5c. In all cases shown in Figs. 3 – 5, the incident wave with the undesired TE polarization is blocked, while the wave with the allowed TM polarization displays a strong resonant transmittance. Away from the frequency of cavity resonance, all the sheet polarizers in Figs. 3 – 5 reflect both the forward and backward propagating waves regardless of its polarization.

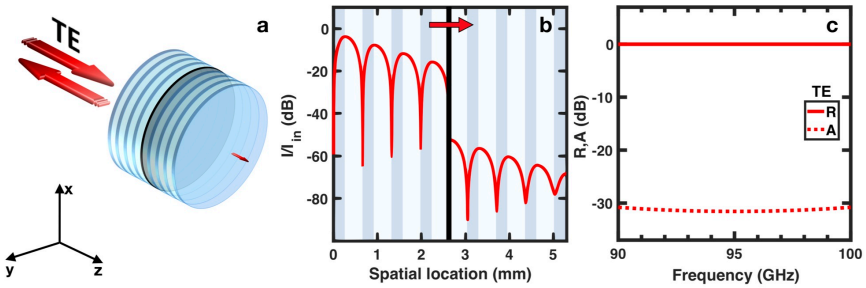

Fig. 3: (a) Schematics of the reflective LSP involving a dichroic nanolayer (black) incorporated into the host structure of Fig. 2a. (b) Simulated spatial intensity distribution, $|E(z)|^2$, of the TE polarization component at 95 GHz; (c) simulated dispersion spectra of the absorptance (A) and reflectance (R) for the TE polarization component.

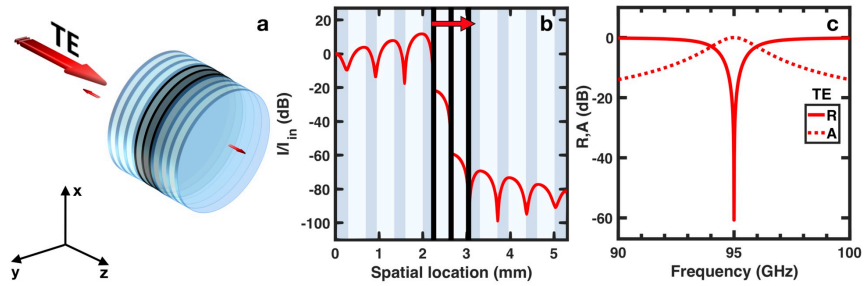

Fig. 4: (a) Schematics of the absorptive LSP involving three dichroic layers (black) incorporated into the host structure of Fig. 2a. (b) Simulated spatial intensity distribution, $|E(z)|^2$, of the TE polarization component at 95 GHz. (c) Simulated dispersion spectra of the absorptance (A) and reflectance (R) of the TE polarization component.

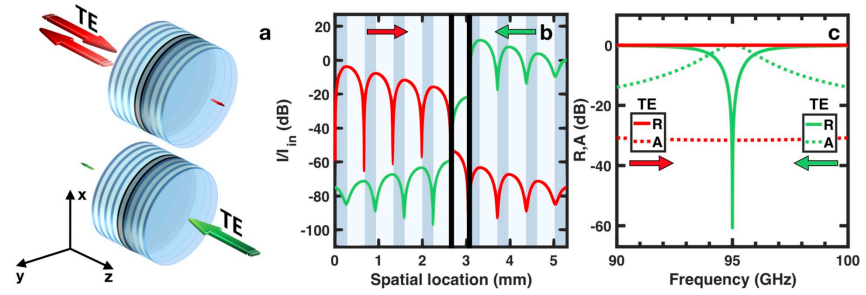

Fig. 5: (a) Schematics of the asymmetric absorptive/reflective LSP involving two dichroic nanolayers (black) incorporated into the host structure in Fig. 2a. (b) Simulated spatial intensity distribution, $|E(z)|^2$, of the TE polarization component for the forward (red) and backward (green) incident waves at 95 GHz. (c) Simulated dispersion spectra of the absorptance (A) and reflectance (R), showing extreme asymmetry with respect to the direction of incidence of the TE polarized input wave.

Note that since the polarizers LSP1 and LSP2 in Fig. 1 are misaligned, the definition of TE (or TM) polarization is polarizer dependent.

As was already pointed, the backward propagating wave passed the Faraday rotator in Fig. 1 must be absorbed by the dichroic sheet polarizer – not reflected back toward the Faraday rotator. The symmetric absorptive configuration in Fig. 4 and the asymmetric reflective/absorptive configuration in Fig. 5, both satisfy the above requirement and thus can be used as components of a sheet isolator. Indeed, the high reflectivity of the TE-polarized wave incident on the front interface of the asymmetric polarizer (the red arrows in Fig. 5) will not compromise the isolator performance. Moreover, the high reflectivity in the latter case will enhance the power capability of the sheet isolator by preventing overheating of the input polarizer LSP1. At the same time, the TE-polarized wave incident on the back interface of the asymmetric polarizer (the green arrows in Fig. 5), does experience nearly perfect resonant absorption, which is essential for the sheet isolator in Fig. 1 to function properly.

As a proof of concept, we fabricated and tested the asymmetric resonant sheet polarizer described above. The LSP was assembled from C-cut sapphire and fused quartz wafers, and aluminum (Al) wire grids deposited on sapphire wafers. The LSP structure is $(S_1Q_1)^2(S_1Q_2)(GS_2)^2(Q_2S_1)(Q_1S_1)^2$, where S_1 and S_2 are 256-μm and 246-μm sapphire, Q_1 and Q_2 are 404-μm and 442-μm quartz, respectively, and G is a 40-nm thick Al wire grid with a duty cycle of 0.3 and periodicity of 20 μm. The design of the LPS was by no means optimized due to limited stock of wafers at the time of assembly.

The wire grid on sapphire (GS_2) was measured with a normally incident gaussian beam in the forward and backward directions. The S-parameters of GS_2 were measured with the use of a Keysight vector network analyzer. We observed no difference between the results obtained for the beams incident in the forward and backward directions, within experimental error. The T and R spectra of the wire grid oriented along the y-axis are shown for the x- and y-polarizations of the incident wave in Fig. 6a and b, respectively. The position of Fabry-Perot resonance of the substrate is indicated by the sharp dip in reflectance R of the x-polarized wave in Fig. 6a. In the vicinity of the resonance, the polarization extinction ratio of the wire grid is about 33 dB. For the rejected y-polarization, the reflectance R is only 0.86, implying that the wire grid still has a significant absorption, $A \approx 0.14$.

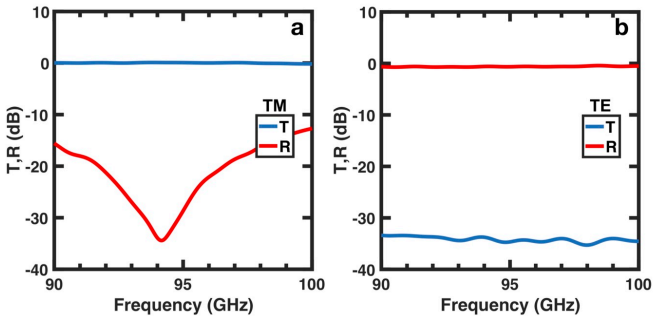

Fig. 6: Transmission characteristics measurements for the wire grid on a sapphire substrate: (a) transmittance (T) and reflectance (R) of the TM polarized wave; (b) T and R for the TE polarized wave.

The same measurements of the S-parameters were carried out for the asymmetric LSP with wire grids being oriented along y-axis. The T and R spectra for the x-polarized wave are shown on Fig. 7a; the difference between the forward and backward directions of incidence in negligible, similar to the case of GS2. The LSP supports perfect resonant transmittance for x-polarization at 94.4 GHz

and is highly reflective away from the resonance, indicating that the grids do not interact with x-polarization component of the radiation. By comparison, the absorbance/reflectance of the y-polarized wave is highly asymmetric, due to its strong interaction with the aluminum grids, as shown on Fig. 7b and 7c. These experimental results are qualitatively identical to the results of our simulations, reflected in Fig. 5c.

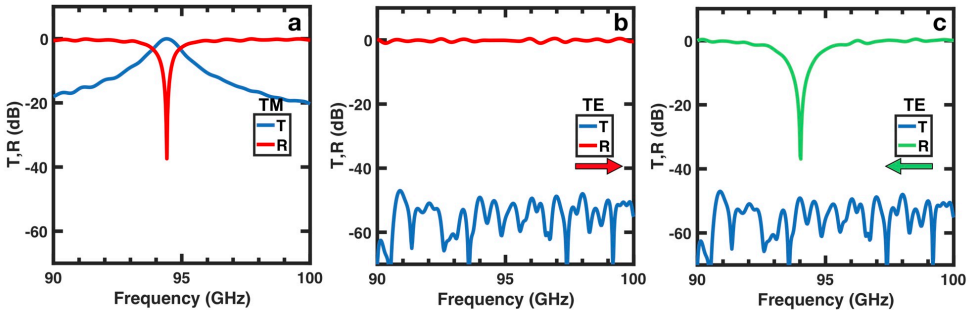

Fig. 7: Transmission characteristics measurements for the asymmetric layered sheet polarizer. (a) Transmittance (T) and reflectance (R) dispersion for the allowed TM polarization. (b) T/R dispersion for the forward propagating wave with the rejected TE polarization (resonant reflection). (c) T/R dispersion for the backward propagating wave with the rejected TE polarization (resonant absorption).

For the forward propagated y-polarized wave measured reflectance R reaches 0.99 at the vicinity of the resonant frequency of 94.4 GHz and transmittance T is suppressed down to -50dB within the entire band gap. This implies that absorptance A of the wave traveling in forward direction is smaller than 0.01. By contrast, for the backward propagated y-polarized wave, the measured reflectance R shows extremely sharp -38 dB dip at 94.03 GHz, with transmittance T being absolutely the same as in the case of forward propagated wave. This indicates that for the y-polarization component of the wave travelling in backward direction the experimental LSP is almost completely absorptive at the resonant frequency.

Note that the Fabry-Perot resonant frequency for the y-polarization incident in backward direction is red-shifted to 94.03 GHz from 94.4 GHz, which can be seen from the difference in position of reflectance R dip in Fig. 7a and 7c. This is attributed to the reactance of the wire grids, which makes their optical thickness for y-polarized component large enough to produce a measurable shift. This effect can be further reduced by lowering periodicity of the grid from 20 μm down to few microns. Demonstrated mm-wave LSP exhibit a large 50dB extinction ratio. The degree of reflection asymmetry for y-polarized light is about 5000 at the resonant frequency. In comparison with stand-alone dichroic nanolayer, the asymmetric LSP offers 20dB higher extinction ratio and significantly enhanced power capabilities (for the forward propagating wave). Also, according to our measurements, if light is incident on the LSP at oblique incidence, its performance will not be significantly affected, as long as the angle of incidence does not exceed 40-degree. The oblique incidence, though, results in a blue-shift of the resonant frequency, which provides ability to tune the operational frequency by tilting the LSP.

Another fundamental problem associated with the existing free-space isolators is that they fail to stop the light obliquely incident on the back interface. Indeed, at oblique incidence, the backward propagating light transmitted by the polarizer LSP2 in Fig. 1 and subsequently by the Faraday rotator, will acquire elliptic polarization and, thus, will not be completely blocked by the polarizer LSP1. One way to address this problem and to make the sheet isolator omnidirectional is to add a metallic nanolayer to the multilayered sheet-isolator. The location of the metallic nanolayer should coincide with the nodal plane of the electric component of the resonant field distribution. At normal

incidence, such a nanolayer is "invisible" for the resonant mode and does not interfere with the resonant transmittance of the allowed linear polarization. At oblique incidence, though, the nodal plane of the electric field distribution shifts away from the metallic nanolayer, and the entire multilayered structure becomes highly reflective at any frequency. For this to happen, the nodal plane location must not coincide with the local symmetry plane (if any) of the multilayered structure. The detail description of this approach can be found in [14]. In the case considered in [14], the metallic nanolayer was ferromagnetic and, thus, it provided not only rejection of obliquely incident light, but also the 45-degree Faraday rotation for the light with normal incidence. In this paper, we will not further elaborate on the problem of oblique incidence.

The most straightforward way to build a sheet isolator is to place a thin-sheet Faraday rotator between a payer of misaligned sheet polarizers, as schematically shown in Fig. 1. A possible design of a resonant thin-sheet Faraday rotator for microwave frequencies was discussed in [14], where a ferromagnetic (cobalt) nanolayer was placed in a nodal plane of the electric component of the quasi-localized mode in a multilayered resonant cavity. Such a configuration allows to drastically suppress the Ohmic losses caused by the cobalt electric conductivity, while, dramatically enhancing the magnetic Faraday rotation. The latter effect is explained as follows. At microwave frequencies, the Faraday rotation is caused by the interaction of oscillating magnetic field with the ferromagnetic material (say, cobalt). Since the nodal plane of the resonant electric field distribution coincides with the antinodal plane of the oscillating magnetic field, we simultaneously have a strong suppression of the Ohmic losses, and a strong enhancement of magnetic Faraday rotation [14].

Here, we suggest the idea of utilizing the same resonant cavity to host the dichroic nanolayers and the magnetic nanolayer responsible for the Faraday rotation. In this case, the polarizers cannot be identified as separate components of the entire stack. Such an integrated design can be seen as an optimized version of the layered sheet-isolator. A numerical example of the integrated sheet-isolator design is presented in Fig. 8. The resonant millimeter-wave cavity is composed of low-loss quartz and sapphire quarter-wave layers. The cavity hosts both magnetic and dichroic layers. The Faraday rotation is provided by a 9.3-μm thick strontium ferrite layer with the permittivity $\epsilon = 2.15 + i0.015$ [20] and Verde constant $v = 1530$ rad/ T·m [21], in a bias magnetic field of 540 mT. The dichroic components are presented by two pairs of 9-nm thick aluminum wire grids with a duty cycle of 0.25. According to our simulations, the integrated sheet-isolator provides the forward resonant transmittance with insertion loss of 3 dB (Fig. 8b, red line). At resonance frequency of 95 GHz, the isolation ratio is about 40 dB (Fig. 8b, green line). Away from the resonance, the entire multilayered structure is highly reflective in either direction.

The integrated sheet-isolator in Fig. 8 supports resonant transmittance for the forward y-polarized incident wave. Dichroic nanolayers in this case do not affect the propagation of the y-polarized wave incident on the front interface (propagating in the forward direction). The x-polarization component of the wave incident on the front interface will not enter the multilayer and will be reflected. The portion of the wave incident on the back interface (propagating in backward direction) that passes through the right-side set of dichroic nanolayers and the magnetic layer, will be subsequently absorbed by the dichroic nanolayers on the left-hand side of the magnetic layer, as clearly seen in Fig. 8d. At the resonant frequency, the isolation ratio of the integrated sheet-isolator in Fig. 8 is predicted to be as high as – 40dB.

In conclusion, let us reiterate that the proposed wide-aperture sheet isolators are based on a low-loss resonant cavity hosting subwavelength dichroic nanolayers and a magnetic layer with normal

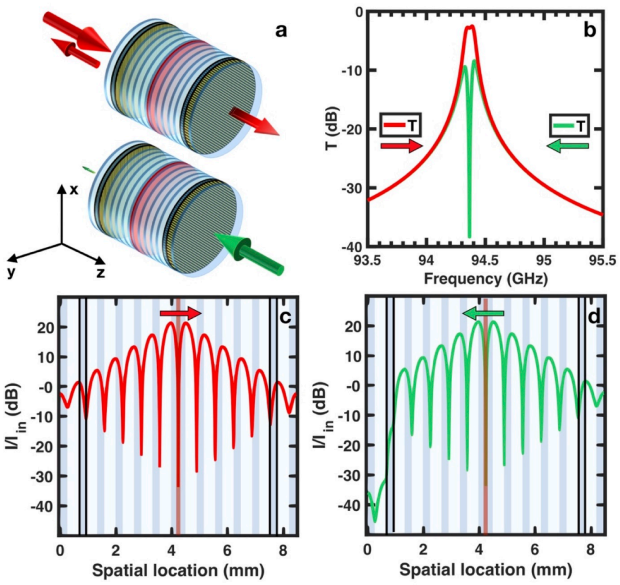

Fig. 8: (a) Schematics of the integrated sheet-isolator composed of quartz (light blue) and sapphire (dark blue) quarter-wave layers, a magnetic layer (red), and two pairs of aluminum wire grids (black). Simulated transmittance dispersion (b) and simulated intensity distribution, $|E(z)|^2$, at the resonance frequency of 94.37 GHz (c and d) for the forward (red) and backward (green) incident waves.

magnetization. The forward transmittance of a sheet isolator is essentially narrowband, due to its resonant nature. The role of the cavity resonance is essential and multifold. Firstly, the resonance enhances the magnetic Faraday rotation produced by a subwavelength magnetic layer, thereby allowing to make the sheet isolator rather thin – its total thickness does not exceed a few wavelengths. Secondly, the resonant conditions allow the use of thin dichroic nanolayers by enhancing/modifying their dichroic properties. In particular, the resonant conditions provide a nearly total (resonant) absorption of the backward propagating light by the dichroic nanolayers, thereby, preventing the sheet isolator from failure. The same dichroic nanolayers taking away from the multilayered resonant cavity would be mostly reflective and, thus, could not be used in a sheet isolator. Finally, the resonant conditions are necessary for the formation of a quasi-nodal plane in the oscillating electric field distribution. Placing a metallic nanolayer at the location of an asymmetric nodal plane results in the rejection of obliquely incident light and rendering the sheet-isolator omnidirectional [14].

2. Reflective photonic limiter for the W-band

Photonic limiters (PLs) are safety devices transmitting low intensity radiation, while blocking electromagnetic radiation with excessively high intensity. The existing passive PLs (those activated by the incoming radiation itself) utilize nonlinear optical materials, which transmit low-intensity radiation while blocking radiation with intensity exceeding a certain limiting threshold [22] (Fig. 9a). The existing PLs, however, have serious limitations in their capacity to provide necessary protection against radiation induced damage. Firstly, the threshold energy for nonlinear behavior is usually higher than practically required values of the limiting threshold. Secondly, the limiting threshold provided by most of the known nonlinear optical materials is not far away from their damage threshold. Thirdly, nonlinear optical properties are frequency dependent; therefore, at certain wavelengths, nonlinear optical materials may not provide protection to optical systems.

To address the above problems, the so-called "reflective" PLs (reflecting rather than absorbing electromagnetic radiation) have been recently developed [23-25] (Fig. 9b). Reflecting PLs are capable of increasing the damage threshold while adjusting the limiting threshold to a required level by incorporating nonlinear optical materials in a resonant photonic structure/cavity [23-25] (Fig. 9b). At low intensity, such a cavity displays a strong resonant transmission. As the input light intensity grows, the nonlinear absorption kicks in, and the entire structure becomes lossy due to

nonlinear absorption enhanced by the cavity resonance. Further increase in light intensity results in total suppression of the resonant mode. As a consequence, the entire layered structure becomes highly reflective (not absorptive!). Importantly, the vulnerable layer with nonlinear absorption is shielded from the high-intensity incident light by one of the Bragg reflectors. The major advantages of the design based on resonant cavity with purely nonlinear absorption include: (i) a significant and controllable reduction in the limiting threshold; (ii) an increase in the limiter damage threshold, due to the shielding of the nonlinear layer; (iii) an orders-of-magnitude reduction in the high-intensity transmittance. On the downside, (i) in the transition range between the low-intensity transmittance and high-intensity reflectance, the resonant cavity will be highly absorptive, much more so than in the case of a single layer made of the same optical material with nonlinear absorption; (ii) due to the resonant nature of the low-intensity transmittance, the above approach essentially requires optical materials with purely nonlinear absorption, because even a small linear absorption will be greatly enhanced at the cavity resonance. Materials with purely nonlinear absorption do exist, but they can only perform at specific frequency ranges.

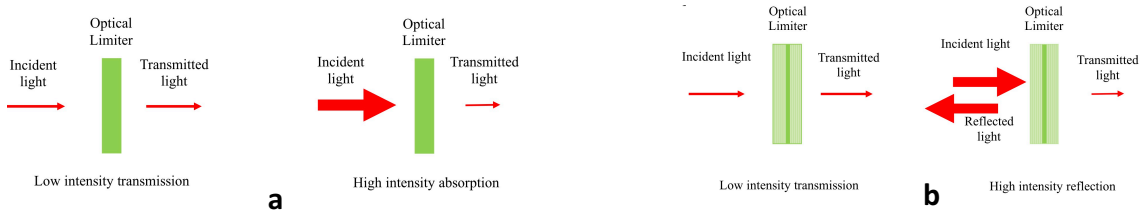

Fig. 9. Schematics of passive absorbing (a) and reflective (b) photonic limiters, transmitting low-intensity radiation while blocking high-intensity radiation.

In principle, the problem with linear absorption can be solved by switching to PLs based on the nonlinear refraction, rather than intensity-dependent absorption. A simple example of the kind is provided by a periodic optical structure composed of two alternating components with matching linear refractive indices, but different nonlinear refraction [26,27]. At low light intensity, the periodic structure is optically uniform, while at high intensity, it can develop photonic band-gaps (PBG) and become reflective at the respective frequencies. A similar idea is to use the intensity-dependent shift of the photonic bands in a PBG structure [28]. A potential advantage of the above approaches is that either of them can provide a broadband low-intensity transmittance. On the downside, (i) the nonlinear shift of the refractive index is usually small, which results in only a narrow-band protection from high-power radiation, as well as inferior attenuation of the high-intensity input; (ii) the direct exposure of nonlinear layers to the high-level input light can negatively affect the limiter damage threshold; (iii) the presence of large number of nonlinear layers can result in highly nonuniform spatial distribution of the high-intensity electromagnetic field inside the photonic structure, which will also negatively affect the performance of the limiter. The above problems can be addressed by using PCMs in which the radiation induced change in the refractive index is significant and abrupt (see, for example Ref. [29]).

In the reported research, we have focused on vanadium dioxide (VO_2), which undergoes transition from the insulating to the metallic phase at 68 ^{0}C. Spectra of transmittance and reflectance (or S-parameters) of a 200-nm VO_2 thin film grown by PLD on a sapphire substrate, measured at 95 GHz in a temperature-controlled environment (Fig. 10a), point to large changes in MW properties of the VO_2 film. The real and imaginary parts of the refractive index of VO_2 extracted from the experimental data are shown in Fig. 10b. These measurements confirm the near-binary nature of

the VO_2 refractive index, which could allow for the low-intensity transmission over a broad temperature range below the transition point. On the other hand, MW losses and heating of VO_2 in the W-band are very small at low temperatures. Indeed, the same VO_2 sample exposed to 95-GHz radiation with power as high as 46 W (gaussian beam, 1.3" FWHM) could not be switch to the high-temperature phase, and therefore requires significant MW absorption enhancement.

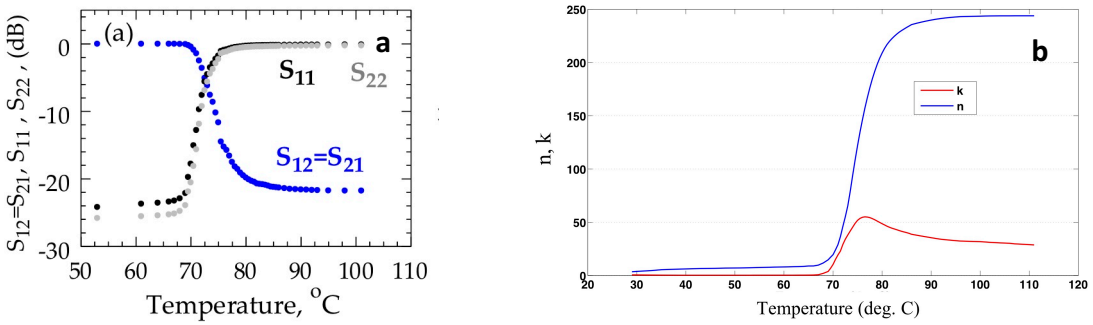

Fig. 10. (a) S-parameters of a 200-nm VO_2 film on sapphire measured at 96 GHz, as a function of temperature (courtesy of M. Hilario, AFRL/RD); (b) real *n* and imaginary *k* parts of the refractive index of the VO_2 film calculated from (a).

Our photonic limiter design [16] is based on a multilayered resonant cavity made of sapphire layers (blue) separated by air gaps (white), incorporating a VO_2 nanolayer (green), as shown in Fig. 11a. The resonator is designed to support a transmission resonance at 95 GHz (Fig. 11b). At the resonance frequency, the electric field distribution (shown in red in Fig. 8a) has an antinodal point at the position of the VO_2 nanolayer. At low intensity radiation and room temperature, the VO_2 nanolayer does not significantly affect the resonant mode and resonant transmission. However, at high intensity radiation the limiter is expected to heat up, to induce the transition in the VO_2 nanolayer from the insulating to the metallic state. In the metallic state, the VO_2 (yellow in Fig. 11c) interacts strongly with the radiation, suppressing the resonant mode along with resonant transmission, resulting in a broadband reflection (Fig. 11d).

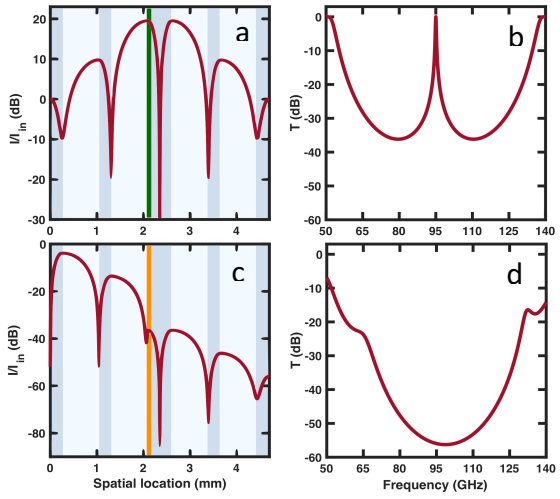

Fig. 11. Photonic limiter for the W-band made of sapphire layers (blue) separated by air gaps (white) and incorporating a VO_2 nanolayer. Spatial distribution of the electric field component of the resonant cavity mode at low (a) and high (c) temperatures; the VO_2 nanolayer is shown in green and yellow, respectively. Resonant transmission (b) and broadband reflection (d) of the photonic limiter at low and high temperatures, respectively.

The photonic limiter design of Fig. 11 was realized with 250-µm sapphire wafers, 780-µm air gaps and a 200-nm VO_2 film deposited on a 525-µm sapphire wafer, and was measured in the temperature-controlled environment. MMW spectra of transmittance (T) and reflectance (R) of the multilayer, as a function of increasing temperature, are shown in Fig. 12. The resonant transmittance peak is seen to initially blue-shift (Fig. 12a) with increasing temperature, and then to completely disappear on reaching temperature of ~74^0 C (Fig. 12b). The multilayer then turns highly reflective (Fig. 12c).

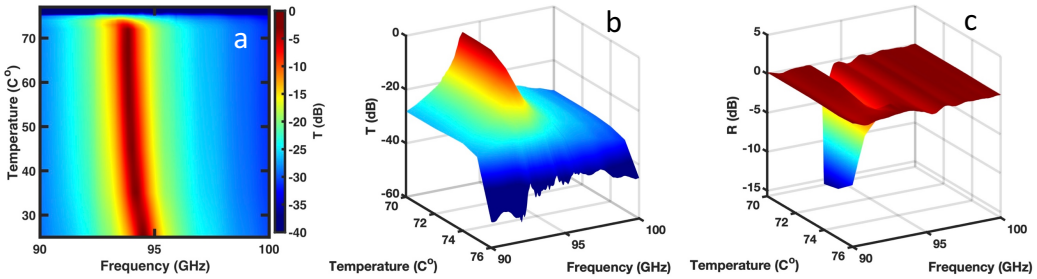

Fig. 12. Transmittance *T*, (a-b) and reflectance *R*, (c) of the multilayer of Fig. 8 as a function of increasing temperature (courtesy of M Hilario, AFRL/RD).

The abrupt changes in the transport characteristics (as in Fig. 12) of the multilayer would be most desirable and productive when the alterations of the refractive index of the VO_2 layer are self-induced. To this end, transmission measurements of the multilayer have been carried out with a high-power source (at 95 GHz) in the ambient air. Once the MMW source has been turned on, the output power was kept at a fixed level (corresponding to incident radiation power of 30, 35, 40, and 46 W) and the absolute transmission was measured as a function of time (Fig. 13).

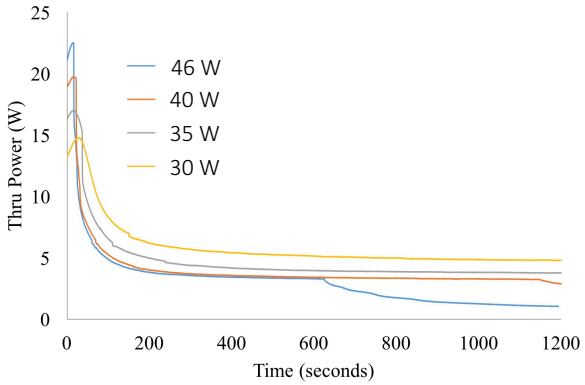

Fig. 13. Transmitted power through the multilayer of Fig. 8, as a function of time, at various incident radiation power, 30, 35, 40, and 46 W.

The presented data have interesting features. Firstly, a sharp drop in transmission at short times, for a fixed incident power, indicates switching of the VO_2 from the insulating to the metallic state. There is clear correlation between the switching time and the incident power: the switching time becomes shorter as the input power increases. The shortest switching time was observed at ~3 s, for a 46 W incident power. Secondly, the drop in transmission (~ 6 dB) is not as large as in that measured in the temperature-controlled environment (~30 dB), at 46 W incident power. And thirdly, the transmission drops to near the same level at longer times, regardless of the incident power.

Notice that the incident beam is gaussian, so that the intensity has a maximum at the center and is falling down from the center. There is then good reason to expect that the phase transition in the VO_2 layer initially occurs at the center of the incident beam and then grows outward from the beam center. Indeed, calculations have shown that gaussian-beam transmission stays the same when the incident power and the (metallic) VO_2 layer area blocking the gaussian beam are both increasing. These are just two competing factors which exactly compensate each other in the measurement.

The evolution in time of the transmission through the multilayer can be better understood with the VO_2 layer imaging, as in Fig. 14. Figs. 14(b-f) are IR images of the forward end of the multilayer at specific times of the transmission in Fig. 11a, indicated by the corresponding vertical dashed lines, for incident power of 46 W. The red spot in the IR images is the metallic phase of VO_2. At incident power of 46 W, initiation (Fig. 14c) and stabilizing (Fig. 14d) of the metallic phase of VO_2 take up to 600 s; the following growth in size of the metallic phase can be explained by heating up of the entire multilayer at later times. Therefore, further investigation of the multilayered PL may require pulsed MMW transmission measurements and Maxwell's-Heat transfer modelling.

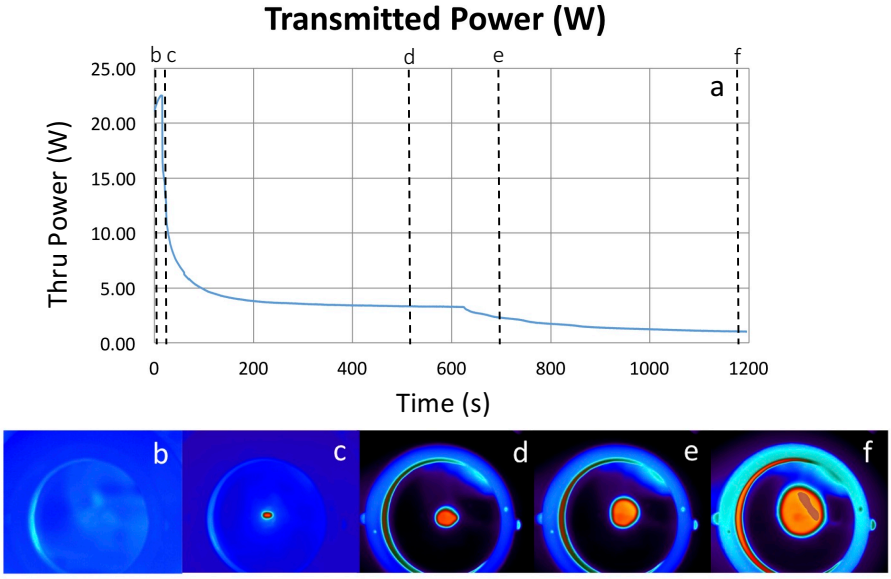

Fig. 14. (a) Evolution in time of the transmission through the multilayer with the VO_2 component for incident power of 46 W; (b-f) IR images of the multilayer at specific times, indicated by the vertical dashed lines in (a).

As in the case of asymmetric metal-dielectric structures [30], one can expect that in the asymmetric PCM-dielectric design, the limiting threshold for the forward propagating light can be different from that for the backward propagating light. Specifically, input light of the same intensity incident from opposite sides of an asymmetric structure can produce different heating effects and, therefore, the transmission coefficient for forward and backward propagation can also be different. The advantages of the approach based on light-induced heating over using asymmetric structures with conventional nonlinear materials can include: (i) a much lower input light intensity required to trigger a change in the temperature-dependent material parameters, and (ii) a change in the complex index being much larger than that of conventional nonlinear effects. For a given PCM layer (VO_2 in our case), the lower and the upper limits of the incident light intensity within which the structure displays unidirectional transmittance, can be engineered by the proper choice of the

layered structure geometry. The frequency of the unidirectional (forward) resonant transmittance can also be changed significantly.

References:

[1] J. D. Joannopoulos, S.G. Johnson, J.N. Winn, R. D. Meade, *Photonic Crystals: Molding the Flow of Light*, (Princeton University Press ,2008).
[2] A. Figotin and I. Vitebskiy, "Electromagnetic unidirectionality in magnetic photonic crystals", *Phys. Rev. B* **67**, 165210 (2003).
[3] A. Figotin and I. Vitebskiy, "Slow wave phenomena in photonic crystals", *Lasers & Photonics Reviews* **5**, 201 (2011).
[4] M. Inoue, K. Arai, T. Fuji, and M. Abe, "Magnetooptical properties of one-dimensional photonic crystals composed of magnetic and dielectric layers", *J. Appl. Phys.* **83**, 6768-6770 (1998).
[5] S. Sakaguchi and N. Sugimoto, "Transmission properties of multilayer films composed of magnetooptical and dielectric materials", *J. Lightwave Technol.* **17**, 1087-1092 (1999).
[6] M. J. Steel, M. Levy, and Jr R. M. Osgood, "Photonic bandgaps with defects and the enhancement of Faraday rotation", *J. Lightwave Technol.* **18**, 1297-1308 (2000).
[7] A. Yariv, Y. Xu, R. K. Lee, and A. Scherer, "Coupled-resonator optical waveguide: a proposal and analysis", *Opt. Lett.* **24**, 711 (1999).
[8] Y. -H. Ye, J. Ding, D. -Y. Jeong, I. C. Khoo, and Q. M. Zhang, "Finite-size effect on one-dimensional coupled-resonator optical waveguides", *Phys. Rev. E* **69**, 056604 (2004).
[9] N. N. Lepeshkin, A. Schweinsberg, G. Piredda, R. S. Bennink, and R. W. Boyd, "Enhanced nonlinear optical response of one-dimensional metal-dielectric photonic crystals", *Phys. Rev. Lett.* **93**, 123902 (2004).
[10] M. Inoue, K. Arai, T. Fuji, and M. Abe, "One-dimensional magnetophotonic crystals", *J. Appl. Phys.* **85**, 5768-5770 (1999).
[11] S. Kahl and A. M. Grishin, “Enhanced Faraday rotation in all-garnet magneto-optical photonic crystals” *Appl. Phys. Lett.* **84**, 1438-1440 (2004).
[12] T. Goto et al., “Optical Tamm states in one-dimensional magnetophotonic structures”, *Phys. Rev. Lett.* **101**, 113902 (2008).
[13] T. Hamon, S. Buil, E. Popova, P. R. Dahoo, and N. Keller, "Investigation of a one-dimensional magnetophotonic crystal for the study of ultrathin magnetic layer", *J. Phys. D: Appl. Phys.* **39**, 1012-1017 (2006).
[14] A.A. Chabanov, K. Smith, T. Carroll, and I. Vitebskiy, “Metal-dielectric photonic structures with extreme directionality: A concept of wide-aperture omnidirectional isolator” (pp. 79 - 81). *8th International Congress on Advanced Electromagnetic Materials in Microwaves and Optics* (Copenhagen, Denmark), 2014/IEEE.
[15] R. Kononchuk, C. Pfeiffer, I. Anisimov, N. Limberopoulos, I. Vitebskiy, and A.A. Chabanov, “Multilayered sheet-polarizers with enhanced polarization ratio and high power tolerance”, submitted to *Physical Review Applied*.
[16] R. Kononchuk, A.A. Chabanov, M. Hilario, B. Jawdat, B. Hoff, V. Vasilyev, N. Limberopoulos, and I. Vitebskiy, “Reflective photonic limiter for the W-band” (pp. 46-48). *11th International Congress on Engineered Materials Platforms for Novel Wave Phenomena* (Marseille, France), 2017/IEEE.
[17] B. Saleh and M. Teich, *Fundamentals of photonics* (2nd ed.) (Hoboken, N.J: Wiley-Interscience, 2007).
[18] Yu, X.J., Kwok, H.S., “Optical wire-grid polarizers at oblique angles of incidence”. *Journal*

of applied physics ***93*****,** pp. 4407-4412, (2003).
[19] Grande, M., Bianco, G.V., Vincenti, M.A., de Ceglia, D., Capezzuto, P., Scalora, M., D'Orazio, A. and Bruno, G., "Optically transparent microwave polarizer based on quasi-metallic graphene". *Scientific reports* ***5***, 17083, (2015).
[20] Korolev, K.A., Subramanian, L. and Afsar, M.N., "Complex permittivity and permeability measurements of ferrite powders at millimeter waves". In *Microwave Conference, 2005 European* (Vol. 2, pp. 3-pp). IEEE.
[21] Shalaby M., Peccianti M., Ozruk Y., Morandoti R., "A magnetic non-reciprocal isolator for broadband terahertz operation," *Nature Communications* **4**, 1558 (2013).
[22] D. J. Hagan, "Optical Limiting", in *Handbook of Optics*, Vol. IV, M. Bass, Ed., (Optical Society of America, 2000).
[23] E. Makri, H. Ramezani, T. Kottos, and I. Vitebskiy*,* "Concept of a reflective power limiter based on nonlinear localized modes"*, Phys. Rev. B* **89**, 031802(R) (2014).
[24] E. Makri, T. Kottos, and I. Vitebskiy*,* "Reflective optical limiter based on resonant transmission"*, Phys. Rev. A* **91**, 043838 (2015).
[25] J. H. Vella, J. H. Goldsmith, A. T. Browning, N. I. Limberopoulos, I. Vitebskiy, E. Makri, and T. Kottos, "Experimental realization of a reflective optical limiter", *Phys. Rev. Appl.* **5**, 064010 (2016).
[26] D. T. Nguyen, C. Sheng, J. Thomas, R. Norwood, B. Kimball, D. M. Steeves, and N. Peyghambarian, "Observation of nonlinear transmission enhancement in cavities filled with nonlinear organic materials", *Appl. Opt*. **47**, 5777 (2008).
[27] X. Zhu, J. Wang, P. Lau, D. Nguyen, R. A. Norwood, and N. Peyghambarian, "Nonlinear optical performance of periodic structures made from composites of polymers and Co_3O_4 nanoparticles", *App. Phys. Lett.* **97**, 093503 (2010).
[28] M. Scalora, J. P. Dowling, C. M. Bowden, and M. J. Bloemer, "Optical limiting and switching of ultrashort pulses in nonlinear photonic band gap materials", Phys. Rev. Lett. 73, 1368 (1994).
[29] Y. Seo, J.-S. Chung, Y. Lee, E. Choi, and B. Cheong, "Spectroscopic investigation on phase transitions for $Ge_2Sb_2Te_5$ in a wide photon energy and high temperature region", *Thin Solid Films* **520**, 3458 (2012).
[30] E. Makri, K. Smith, A. Chabanov, I. Vitebskiy, and T. Kottos, "Hypersensitive transport in photonic crystals with accidental spatial degeneracies", *Sci. Rep.* **6**, 22169 (2016).